Temperature Dependence of Structure Parameters in Natural Magnetite: Single Crystal X-ray Studies from 126 to 773 K

H. OKUDERA,[a]* K. KIHARA[b] AND T. MATSUMOTO[b]

[a]*Department of Science for Natural Environment, Graduate School of Natural Science and Technology, Kanazawa University, Kakuma-machi, Kanazawa 920-11, Japan, and* [b]*Department of Earth Sciences, Faculty of Science, Kanazawa University, Kakuma-machi, Kanazawa 920-11, Japan. E-mail: okudera@kenroku.ipc.kanazawa-u.ac.jp*

Abstract

Structural parameters and their thermal changes in natural magnetite, Fe_3O_4, have been studied using the single crystal X-ray diffraction method in the temperature range 126–773 K. The cell dimensions, oxygen coordinate and atomic mean square displacements (m.s.d.'s) reversibly change as a function of temperature. The coordinate of oxygen remains almost constant at $x = 0.2549$ (1) below ~600 K, but increases with increasing temperature above this temperature. This characteristic behavior of the oxygen coordinate with temperature indicates that the cation disordering over the tetrahedral (A) and octahedral (B) cation sites occurs above 600 K. All atomic m.s.d.'s increase monotonously with temperature rise. The m.s.d.'s of the B atom show a unique temperature dependence. At lower temperatures the B atom prefers to vibrate along [111], but this preference is reduced with a temperature rise up to 630 K, above which the m.s.d. normal to [111] becomes dominant.

1. Introduction

At room temperature magnetite is a mixed-valence iron oxide with the spinel structure (Fig. 1) and its space group has been redetermined as $Fd\bar{3}m$ (Fleet, 1986). The spinel structure with space group $Fd\bar{3}m$ consists of three atomic sites, $8(a)$ $\bar{4}3m$, $16(d)$ $.\bar{3}m$, and $32(e)$ $.3m$ (no. 227 in *International Tables for Crystallography*, 1987, Vol. A). In oxide spinels O atoms occupy the position $32(e)$ (O site) with coordinates (x, x, x) and form cubic close-packing. We use x as the oxygen coordinate parameter rather than u, as often used, to avoid confusion with the m.s.d. of an atom, $\langle u^2 \rangle$, in this paper. When the origin of the structure was fixed at the center of symmetry [$16(c)$ $.\bar{3}m$, origin choice 2], the x value for magnetite is almost 0.2548 at room temperature (*e.g.* Hamilton, 1958; Fleet, 1986), which is larger than 0.25 for the closest packing. Cations occupy the tetrahedral (A site) and octahedral interstices (B site) of close-packed O atoms, at positions $8(a)$ and $16(d)$, respectively. BO_6 octahedra share their edges with each other and are arrayed along <110>.

Taking i to be the degree of inversion (inversion parameter), an oxide spinel XY_2O_4 is expressed as

$^{iv}(X_{(1-i)}Y_{(i)})$ $^{vi}[X_{(i)}Y_{(2-i)}]$ O_4. Note that perfectly normal, inverse (both ordered) and random arrangements of cations correspond to $i = 0, 1$ and 2/3, respectively. If magnetite is an ionic crystal, its ideal structural formula at room temperature is $^{iv}Fe^{3+}[^{vi}Fe^{2+}$ $^{vi}Fe^{3+}]O_4$, which is the 2–3 inverse type of cation distribution ($i = 1$). However, ionic interpretation of the magnetite structure is highly controversial (*e.g.* Todo, Siratori & Kimura, 1995). Measurements of thermal change of electrical resistivity of magnetite (Todo *et al.*, 1995) suggest band character in electron transport between the B-site cations and semimetallic character above the Verwey transition temperature ($T_V \simeq 120$ K).

In some spinels, x and i are closely related with each other and change as a function of temperature (*e.g.* $MgAl_2O_4$ by Peterson, Lager & Hitterman, 1991). In magnetite, Wu & Mason (1981) measured the Seebeck coefficient and derived the i value as a function of temperature in the range 873–1773 K. From their equilibrium constant for cation distribution, the i value at 873 K is calculated as 0.86, corresponding to 41% of cation disordering. On the other hand, no precise determination of x with varying temperature has been reported. Charge disordering over a common nucleus at a high temperature is unquenchable and then an *in situ* observation is required to investigate the change of x, and the relation between x and i, in magnetite.

In this study we investigated temperature dependence of the structure parameters of natural magnetite in the temperature range 126–773 K, using *in situ* X-ray single crystal diffraction data. The possibility of charge-disordering between the A and B sites will be discussed using these parameters.

2. Experimental

2.1. *Specimens*

Experiments were performed on natural crystals from chlorite schist of Nagatoro, Saitama Pref., Japan These crystals occur as euhedral octahedral grains, usually less than 2 mm in [100], in the chlorite schist. In these crystals, sphene ($CaTiSiO_4$) is found as a very minor inclusion with irregular shape under SEM

(scanning electron microscopy) observation. Impurities were determined as 0.13 wt % of MnO, 0.03 wt % of MgO and 0.02 wt % of TiO_2 in electron microprobe analysis. Si, Al, Cr, Ni and Ca were not detected. The average cation deficiency was determined as 1.07% by measuring the weight gain of the crystals after oxidation to Fe_2O_3 by heat treatment up to 1273 K in air. Calculated crystal data at 299 K are: $Fe^{3+}_{2.0486}Fe^{2+}_{0.9131}Mn_{0.0042}Mg_{0.0017}Ti_{0.0006}\square_{0.0318}O_4$, M_r = 229.70, V = 591.12 (3) $\mathring{A}^3$, D_c = 5.162 g cm^{-3}, Z = 8, $F(000)$ = 873.16. The occurrence of the Verwey transition was confirmed in the temperature range 110–125 K by observing a sudden alteration in the temperature dependence of the magnetization. Thus,

diffraction intensity measurements were carried out at temperatures down to 126 K.

The two specimens (numbers 7 and 14) were selected from regular octahedral crystals and used in the X-ray intensity measurements. These crystals were all confirmed to be single phases by Weissenberg photographs; no extra diffraction peaks attributable to sphene were observed. They were ground into spheres having diameters of 0.24 (number 7) and 0.145 mm (number 14) and sealed into evacuated silica glass capillaries without adhesive.

2.2. Low-temperature experiments

Diffraction intensities and θ angles were measured on specimen number 14 mounted on a Rigaku AFC-5S automated four-circle diffractometer with a Rigaku N_2 gas-flow cooling device. Temperature fluctuations near the nozzle inside the Dewar tube were less than 1 K during measurements and the total uncertainty of temperature measurements was estimated to be less than 5 K. Intensity data were collected using the ω–2θ scan mode [scan width $\omega = (1.5 + 0.35\tan\theta)°$] with graphite-monochromatized Mo $K\alpha$ radiation (λ = 0.71069 Å) in the temperature range 126–297 K. The experiments were performed in the cooling-and-heating cycle to check the presence of hysteresis on the structural parameters. Reflections with $h \geq 0$, $k \geq 0$, $l \geq 0$ and their Friedel pairs for the cooling cycle and half those (with the further condition $|l| \geq |k|$) for the heating cycle were measured up to $2\theta = 100°$. Measured intensities showed no remarkable thermal change in the temperature range above 148 K, whereas they showed large differences at 126 K in comparison to those at 148 K. The cell dimension was determined with θ values measured by the half-shutter method. Results of the least-squares fitting for the cooling cycle using 20–25 of the most
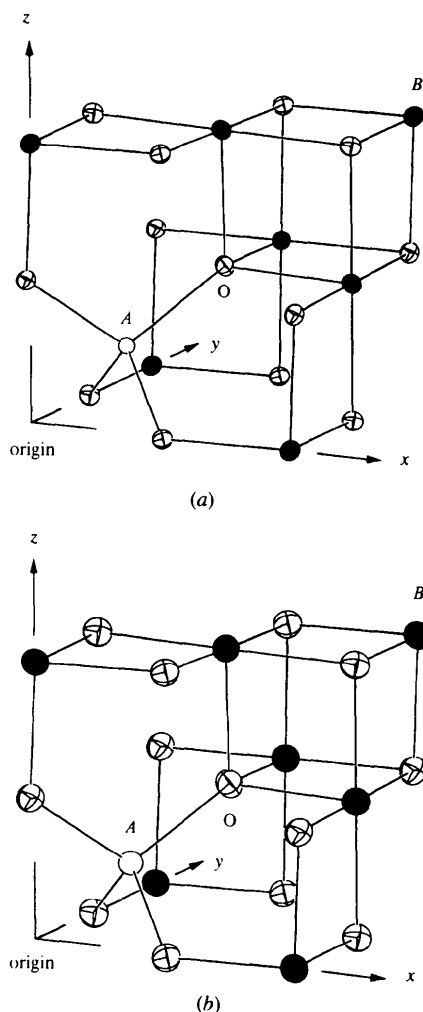

Fig. 1. ORTEP drawings (Johnson, 1971) of the structure of magnetite, showing the designation of atoms and crystallographic axes with their origin at the center ($.\bar{3}m$). Open circle: tetrahedral cation (A-site cation); hatched ellipsoids: octahedral cations (B-site cations); open ellipsoids: oxygens (O). Each circle and ellipsoid represent a 50% probability ellipsoid obtained in the present refinements. One-eighth of a cell, $x \simeq 0-\frac{1}{2}$, $y \simeq 0-\frac{1}{2}$, $z \simeq 0-\frac{1}{2}$, is shown: (a) 299 and (b) 773 K.
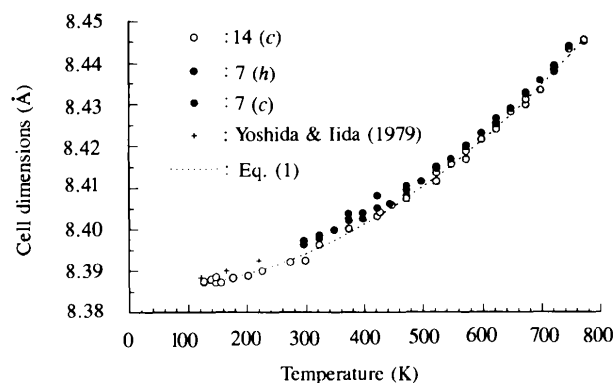

Fig. 2. Temperature variation of the cell dimension between 126 and 773 K. Open circles: cooling cycle on number 14; hatched circles: heating cycle on number 7; solid circles: cooling cycle on number 7. Difference between results of cooling and heating cycles on number 14 are negligible and only those in the cooling cycle are drawn. Error bars (1σ) are hidden behind the circles. Data taken from Yoshida & Iida (1979) are shown with crosses. The dashed line corresponds to equation (1).

intense peaks in $50 < 2\theta < 80°$ are shown in Fig. 2. A list of observed cell dimensions has been deposited.*

2.3. High-temperature experiments

A Philips PW1100 automated four-circle diffractometer, equipped with an electric resistance heater, was used. The heater was controlled by a PID controller with a Pt–PtRh thermocouple in fluctuation less than ± 2 K at 773 K. Two coiled heaters were installed in a steel block, which surrounds the specimen, to make their inducing magnetic field antiparallel. Intensity data were collected in the temperature range 296–773 K on number 7 in the heating-and-cooling cycle. Reflections were measured with the conditions $h \geq k \geq l \geq 0$, $k \geq l \geq h \geq 0$, $l \geq h \geq k \geq 0$ and their Friedel pairs for 2θ up to 86° (up to 88° only at 299 K). The radiation and scan modes were the same as those for the low-temperature experiments. The cell dimension was determined by a least-squares fitting on the centroids of peak profiles measured using the Bond method (Bond, 1960). The cell dimensions determined are shown in Fig. 2. The list of observed cell dimensions has been deposited.*

2.4. Crystal structure refinement

The intensity data were corrected for Lp and absorption ($\mu = 14.22$ mm^{-1} at 299 K) factors. Large deviations among the equivalent reflections were observed in some weak reflections during the data collection. In ψ scanning experiments at room temperature, intensity enhancement was observed for some weak reflections and also some $Fd\bar{3}m$-forbidden reflections, as reported by Fleet (1986). Observed intensities of these anomalous reflections were ψ-sensitive and the intensities of the $Fd\bar{3}m$-forbidden reflections remained at the background level for some ψ angles. Thus, the space group $Fd\bar{3}m$ with its origin at the center of symmetry ($.\bar{3}m$) was chosen for the present magnetite and reflections with $|F|_{max} > 2|F|_{min}$ were excluded from each data set, where $|F|_{max}$ and $|F|_{min}$ are the maximum and minimum intensities of the equivalent reflections, respectively.

Unweighted mean values of the equivalent reflections with $|\bar{F}_{obs}| > 3\sigma(|\bar{F}_{obs}|)$ (σ based on counting statistics) were used in structure refinements. Numbers of independent reflections used for the refinements are given in Tables 1–5. The least-squares program ORXFLS4, the 1977 version of ORFLS (Busing, Martin & Levy, 1962), was used for the refinements with 10 variables, including one scale and one isotropic extinction factor (type I of Coppens & Hamilton, 1970). The weights for $|\bar{F}_{obs}|$ were $1/\sigma^2(|\bar{F}_{obs}|)$ in the refinements. Neutral form factors and anomalous dispersion terms of the

---

* Lists of the observed cell dimension, atomic mean square displacements, interatomic distances, polyhedral volumes and ratios, and structure factors have been deposited with the IUCr (Reference: OH0051). Copies may be obtained through The Managing Editor, International Union of Crystallography, 5 Abbey Square, Chester CH1 2HU, England.

atoms were taken from Tables 2.2A and 2.3.1 of *International Tables for X-ray Crystallography* (1974, Vol. IV). The site occupancy for the O site was fixed at 100%. Because the amount of cation deficiency changes as a function of both temperature and oxygen partial pressure (Dieckmann, 1982), the possibility of changing chemical composition must be taken into consideration. Thus, we varied the site occupancy parameters in the least-squares cycles and monitored them as an indicator of changing composition. The structure refinements were also made with compositional constraint applying the weight-gain measurement data, namely 99% of site occupancies for both cation sites. The structure refinements without constraint converged at smaller values for the site occupancy parameters than those determined by the weight-gain measurement and this reduction commonly occurred for all data sets. In spite of this compositional constraint, refined parameters showed coincidence between these two calculations within 2 e.s.d.'s. These reductions in the site occupancy parameters might arise from the use of neutral form factors. Thus, we present the refined site occupancy parameters in Tables 1–5 to show no notable compositional change during the higher temperature experiments. Finally, the refinements converged to wR, ranging from 0.01 to 0.02 for the two specimens. Lists of structure factors after the final stage of structure refinements have been deposited.*

3. Results

3.1. Cell dimension

The cell dimensions at room temperature (Table 1) agree with those of natural specimens reported by previous authors (Hamilton, 1958; Fleet, 1981, 1982a), but smaller than the synthesized sample (Yoshida & Iida, 1979). Observed cell dimensions for specimen number 14 in the cooling cycle and those for specimen number 7 in the heating cycle, both from room temperature, were fitted using a single second-order polynomial equation (1) with the square of the multiple correlation coefficient $R^2 = 99.8\%$, which was used to obtain the dashed line given in Fig. 2

$$a(\text{Å}) = 8.3856\,(7) - 2\,(4) \times 10^{-6}T + 1.03\,(4) \times 10^{-7}T^2,$$
$$(1)$$

where T is absolute temperature. The linear thermal expansion coefficient α_T ($= a'/a$) derived from (1) is mostly linear in the temperature range examined and generally agrees with the α_T value in the temperature range 314–843 K, reported by Sharma (1950), by means of an interferometer and that obtained by a single third-order polynomial fitting of the change of cell dimensions in the temperature range 122–295 K for the synthetic specimen (Yoshida & Iida, 1979).

---

* See deposition footnote.

Table 1. Structure parameters of magnetites at room temperature in comparison to a previous report

Structure parameters were refined with neutral form factors. The origin of the structure was fixed at the center of symmetry. x indicates the coordinate of oxygen. Thermal parameters were refined in the form

$$T = \exp[-(\beta_{(11)}h^2 + \beta_{(22)}k^2 + \beta_{(33)}l^2 + 2\beta_{(12)}hk + 2\beta_{(13)}hl + 2\beta_{(23)}kl)].$$

The site symmetries give the constraints: $\beta_{(11)} = \beta_{(22)} = \beta_{(33)}$, $\beta_{(12)} = \beta_{(13)} = \beta_{(23)}$, $\beta_{(12)} = 0$ at site A. Thermal parameters of Fleet (1986), presented as B_{ij}, were divided by $4a^2$. e.s.d.'s (1σ) are in parentheses.

		Number 14 (273 K)*	Number 14 (297 K)†	Number 7 (299 K)‡	Number 7 (296 K)§	644C¶
	a (Å)	8.3922 (3)	8.3956 (3)	8.3925 (7)	8.3969 (5)	8.3941 (7)
	Extinction**	0.241 (8)	0.258 (8)	0.252 (14)	0.048 (6)	
A	Occupancy (%)	96.2 (4)	96.3 (4)	97.6 (9)	96.9 (9)	100
$8(a)\,\bar{4}3m$	$\beta_{(11)}(\times10^5)$	140 (3)	153 (3)	175 (4)	177 (4)	123 (4)
B	Occupancy (%)	96.6 (4)	96.7 (4)	98.5 (9)	98.0 (8)	100
$16(d).\bar{3}m$	$\beta_{(11)}(\times10^5)$	192 (2)	205 (2)	225 (3)	235 (3)	165 (4)
	$\beta_{(12)}(\times10^5)$	20 (3)	20 (3)	20 (2)	19 (3)	17 (1)
O	x	0.25484 (11)	0.25488 (11)	0.25487 (10)	0.25492 (12)	0.25486 (8)
$32(e).3m$	$\beta_{(11)}(\times10^5)$	224 (6)	235 (6)	240 (9)	259 (9)	192 (6)
	$\beta_{(12)}(\times10^5)$	−16 (9)	−17 (9)	−19 (8)	−27 (10)	−16 (4)
N_{meas}††		1570	895	816	792	2565
N_{used}‡‡		125	131	103	99	147
R_{int} (%)		1.72	1.62	1.34	1.72	
R (%) §§		1.04	1.16	1.29	1.31	2.2
wR (%) ¶¶		1.03	1.07	1.43	1.60	2.4
S***		0.78	0.76	0.56	0.59	1.8

* Before cooling. † After cooling. ‡ Before heating. § After heating. ¶ Fleet (1986), for natural specimen. ** Isotropic extinction factor for type I extinction (Coppens & Hamilton, 1970). †† Total number of measured reflections. ‡‡ Number of independent reflections used in structure refinements. §§ $R = [\Sigma||F_o| - |F_c||]/\Sigma|F_o|$. ¶¶ $wR = [\Sigma w(|F_o| - |F_c|)^2/\Sigma wF_o^2]^{1/2}$. *** $S = [\Sigma w(|F_o| - |F_c|)^2/r_o - p_{varied}]^{1/2}$, where r_o and p_{varied} are numbers of reflections and varied parameters, respectively.

Table 2. Refined structure parameters of magnetite, number 14 in cooling cycle

	Temperature	126 K	148 K	177 K	226 K
	a (Å)	8.3874 (3)	8.3879 (4)	8.3883 (3)	8.3900 (5)
	Extinction	0.168 (6)	0.259 (7)	0.259 (7)	0.248 (7)
A	Occupancy (%)	97.0 (4)	96.5 (4)	96.2 (4)	96.1 (3)
	$\beta_{(11)}(\times10^5)$	92 (3)	102 (2)	110 (2)	126 (2)
B	Occupancy (%)	97.0 (4)	96.6 (3)	96.6 (3)	96.3 (3)
	$\beta_{(11)}(\times10^5)$	134 (2)	145 (2)	154 (2)	171 (2)
	$\beta_{(12)}(\times10^5)$	30 (2)	31 (2)	28 (2)	23 (2)
O	x	0.25506 (1)	0.25484 (9)	0.25484 (9)	0.25487 (8)
	$\beta_{(11)}(\times10^5)$	170 (6)	174 (5)	182 (5)	207 (5)
	$\beta_{(12)}(\times10^5)$	−6 (8)	−16 (7)	−16 (7)	−14 (7)
	N_{meas}	978 *	1586	1584	1570
	N_{used}	134	131	133	129
	R_{int} (%)	2.28	1.72	1.77	1.83
	R (%)	1.20	0.99	0.98	0.86
	wR (%)	1.06	0.90	0.95	0.85
	S	0.77	0.65	0.68	0.63

* Some intensities were lost by accident at data collection.

Table 3. Refined structure parameters of magnetite, number 14 in heating cycle

	Temperature	148 K	174 K	225 K	274 K
	a (Å)	8.3874 (3)	8.3890 (3)	8.3903 (3)	8.3932 (3)
	Extinction	0.278 (9)	0.273 (10)	0.271 (9)	0.264 (9)
A	Occupancy (%)	96.0 (4)	96.0 (5)	95.6 (4)	96.0 (4)
	$\beta_{(11)}(\times10^5)$	100 (3)	109 (3)	126 (3)	141 (3)
B	Occupancy (%)	96.3 (4)	96.5 (4)	96.1 (4)	96.3 (4)
	$\beta_{(11)}(\times10^5)$	145 (2)	153 (3)	172 (2)	191 (2)
	$\beta_{(12)}(\times10^5)$	30 (2)	27 (3)	26 (3)	20 (3)
O	x	0.25491 (10)	0.25484 (11)	0.25476 (11)	0.25488 (11)
	$\beta_{(11)}(\times10^5)$	173 (6)	184 (7)	209 (6)	222 (6)
	$\beta_{(12)}(\times10^5)$	−19 (7)	−14 (9)	−20 (9)	−22 (9)
	N_{meas}	902	900	902	895
	N_{used}	133	135	134	131
	R_{int} (%)	1.49	1.56	1.62	1.55
	R (%)	1.05	1.18	1.21	1.16
	wR (%)	1.05	1.22	1.15	1.11
	S	0.75	0.87	0.81	0.80

Table 4. *Refined structure parameters of magnetite, number 7 in heating cycle*

Temperature	373 K	473 K	523 K	573 K	623 K	673 K	723 K	773 K
a (Å)	8.4001 (5)	8.4078 (7)	8.4127 (8)	8.4179 (6)	8.4245 (4)	8.4305 (4)	8.4386 (4)	8.4454 (5)
Extinction	0.246 (18)	0.272 (16)	0.288 (15)	0.251 (16)	0.156 (11)	0.123 (10)	0.097 (9)	0.073 (11)
A Occupancy (%)	96.6 (12)	98.4 (10)	98.1 (9)	97.9 (11)	98.1 (10)	97.1 (9)	97.2 (9)	97.0 (13)
$\beta_{(11)}$ (×10^5)	193 (5)	236 (5)	258 (4)	281 (5)	302 (5)	319 (5)	347 (5)	385 (7)
B Occupancy (%)	98.6 (11)	98.9 (9)	98.9 (9)	98.9 (10)	98.8 (9)	98.3 (9)	98.2 (9)	98.1 (12)
$\beta_{(11)}$ (×10^5)	257 (4)	297 (3)	321 (3)	351 (4)	373 (4)	396 (4)	424 (4)	460 (6)
$\beta_{(12)}$ (×10^5)	16 (3)	8 (3)	7 (3)	5 (3)	4 (3)	−8 (3)	−10 (3)	−16 (5)
O x	0.25453 (13)	0.25482 (11)	0.25486 (11)	0.25470 (12)	0.25478 (12)	0.25500 (12)	0.25505 (13)	0.25515 (19)
$\beta_{(11)}$ (×10^5)	270 (11)	312 (10)	344 (9)	373 (11)	397 (10)	418 (10)	457 (11)	481 (16)
$\beta_{(12)}$ (×10^5)	−18 (11)	−29 (10)	−19 (9)	−33 (11)	−44 (11)	−30 (11)	−33 (12)	−31 (18)
N_{meas}	792	798	798	798	798	798	798	798
N_{used}	100	96	97	96	99	97	96	94
R_{int} (%)	1.53	1.30	1.40	1.49	1.60	1.52	1.61	1.83
R (%)	1.39	1.16	1.14	1.37	1.27	1.34	1.30	1.84
wR (%)	1.87	1.50	1.40	1.65	1.62	1.62	1.62	2.34
S	0.72	0.58	0.53	0.62	0.59	0.59	0.57	0.81

Table 5. *Refined structure parameters of magnetite, number 7 in cooling cycle*

Temperature	323 K	373 K	423 K	473 K	523 K	573 K	623 K	673 K	723 K
a (Å)	8.3980 (3)	8.4030 (4)	8.4067 (4)	8.4101 (4)	8.4150 (4)	8.4201 (3)	8.4261 (4)	8.4327 (3)	8.4386 (4)
Extinction	0.050 (7)	0.050 (7)	0.048 (7)	0.056 (8)	0.056 (7)	0.057 (7)	0.059 (7)	0.058 (7)	0.057 (7)
A Occupancy (%)	97.4 (9)	97.7 (9)	97.4 (10)	97.1 (10)	97.6 (10)	97.5 (9)	97.6 (9)	97.3 (9)	97.4 (9)
$\beta_{(11)}$ (×10^5)	191 (4)	209 (5)	225 (5)	252 (5)	264 (5)	291 (5)	314 (5)	334 (5)	354 (5)
B Occupancy (%)	98.0 (9)	98.4 (9)	98.4 (9)	97.9 (10)	98.7 (9)	98.2 (8)	98.3 (9)	98.0 (9)	98.1 (9)
$\beta_{(11)}$ (×10^5)	246 (3)	266 (3)	288 (4)	307 (4)	335 (4)	361 (4)	385 (4)	404 (4)	428 (4)
$\beta_{(12)}$ (×10^5)	17 (3)	18 (3)	17 (4)	9 (3)	8 (3)	2 (3)	2 (3)	−5 (3)	−11 (3)
O x	0.25492 (12)	0.25491 (12)	0.25480 (13)	0.25501 (14)	0.25487 (13)	0.25494 (12)	0.25497 (13)	0.25488 (14)	0.25512 (13)
$\beta_{(11)}$ (×10^5)	276 (10)	286 (10)	306 (10)	337 (11)	353 (11)	382 (10)	403 (10)	445 (11)	468 (11)
$\beta_{(12)}$ (×10^5)	−27 (10)	−36 (11)	−37 (11)	−39 (12)	−39 (12)	−32 (12)	−45 (12)	−45 (13)	−41 (13)
N_{meas}	798	798	797	798	798	798	798	796	845 *
N_{used}	95	95	94	97	96	95	95	94	95
R_{int} (%)	1.62	1.62	1.69	1.81	1.71	1.74	1.84	1.78	1.96
R (%)	1.25	1.24	1.39	1.49	1.41	1.29	1.38	1.37	1.35
wR (%)	1.55	1.59	1.67	1.78	1.71	1.57	1.60	1.66	1.64
S	0.58	0.59	0.62	0.64	0.61	0.56	0.56	0.58	0.56

* Some intensities were doubly measured by accident at data collection.

3.2. Structure parameters

The structure parameters at room temperature are listed and compared with those of Fleet (1986) in Table 1 and those at various temperatures are presented in Tables 2–5. The thermal change of the oxygen coordinate x and cation–anion bond lengths are shown in Figs. 3 and 4, respectively. Observed m.s.d.'s of the *A*-, *B*- and O-site atoms (abbreviated as *A*, *B* and O atoms, respectively) along the principal axes of the thermal vibrational ellipsoids are shown in Fig. 5 for selected cycles. Lists of m.s.d.'s of atoms, selected interatomic distances, polyhedral volumes and their ratios have been deposited.*

No remarkable hysteresis was observed in the refined structural parameters between the heating-and-cooling cycles. The oxygen coordinate x at room temperature is in good agreement with those reported by previous authors (Hamilton, 1958; Fleet, 1986). The x values in the temperature range 148–573 K are virtually constant at 0.2549 with standard deviation 0.0001. The x values increase above 600 K with increasing temperature. The increase of x is reflected more clearly in

the *A*—O distance than the *B*—O distance (Fig. 4): the former [abbreviated as $R(A$—O)] steadily increases with increasing temperature, but its slope increases rapidly at ~550 K, whereas the temperature dependence of the latter [abbreviated as $R(B$—O)] is linear within the range of the present experiments.

4. Discussion

The positive electron density at the interstitial site, the equipoint 8(b), noted by Fleet (1981, 1986), also appeared in the present difference-Fourier syntheses. This residue, however, vanished with the use of different isotropic extinction corrections by Becker & Coppens (1974), whereas strong positive residues remained at the *A*, *B* and O sites other than the 8(b) site. Therefore, the positive residue at the 8(b) site observed in one of our difference-Fourier maps is not enough to lead us to an additional structure feature such as interstitial cations.

4.1. Thermal change of anisotropic thermal vibrations of atoms

The temperature factors of the *B* atom in magnetite are more strongly anisotropic at room temperature

than in other spinels (*e.g.* Yagi, Marumo & Akimoto, 1974; Morimoto, Tokonami, Watanabe & Koto, 1974; Marumo, Isobe & Akimoto, 1977; Yamanaka, Takéuchi & Tokonami, 1984; Yamanaka, 1986). At lower temperatures, displacements along [111] predominate over those in the directions normal to [111]. The thermal vibrational ellipsoid for the *B* atom changes its shape from prolate spheroidal to oblate spheroidal around [111] with increasing temperature: the ratio of m.s.d.'s in the two directions is 1.8:1 at 148 K and 0.9:1 at 773 K. The crossover point of these two m.s.d.'s is at ~630 K in both the heating and cooling cycles. Even though the anharmonic terms in atomic motion with the Gram–Charlier expansion equation (Johnson & Levy, 1974) were included in the least-squares calculations, these higher-order terms were insignificant at lower temperatures.

The thermal ellipsoid of the O atom is oblate spheroidal with the shortest principal axis along the direction of the *A*—O bond, as observed in other spinels (*e.g.* Yagi *et al.*, 1974; Morimoto *et al.*, 1974; Marumo *et al.*, 1977; Yamanaka *et al.*, 1984; Yamanaka, 1986). Two sets of values for m.s.d.'s are plotted in Fig. 6
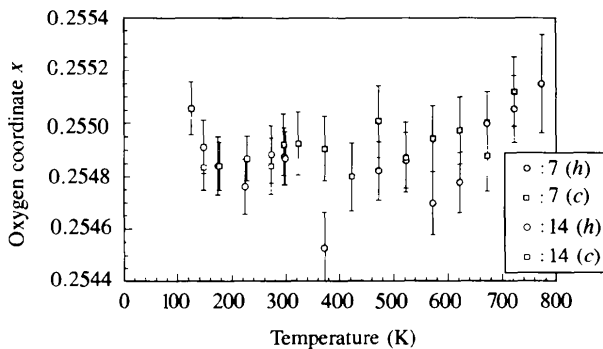
for selected cycles: one is the difference along the bond, $\Delta<u^2>_{(O—A)\parallel} = <u^2>_{(O)\parallel} - <u^2>_{(A)\parallel}$, and the other along the direction normal to the bond, $\Delta<u^2>_{(O—A)\perp} = <u^2>_{(O)\perp} - <u^2>_{(A)\perp}$. As seen in Fig. 6, $\Delta<u^2>_{(O—A)\perp}$'s are larger than $\Delta<u^2>_{(O—A)\parallel}$'s, which are almost null or below 2×10^{-3} Å^2. These features observed in thermal

(a)

(b)

(c)

Fig. 5. Changes in m.s.d.'s ($<u^2>$) at each atomic site, along the principal axes of their thermal vibrational ellipsoids. The difference between results of heating and cooling cycles are negligible and selected cycles are drawn. Error bars (1σ) are hidden behind symbols at some data points. Letters in parentheses with subscripts p and n, if denoted, designate m.s.d.'s for each atom in directions parallel and normal to [111], respectively. Open circles and triangles: cooling cycle on number 14; hatched circles and triangles: heating cycle on number 7. (*a*) *A* site, (*b*) *B* site and (*c*) O site.

Fig. 3. Change in *x* as a function of temperature; *h*: heating cycle; *c*: cooling cycle. Error bars represent 1σ.
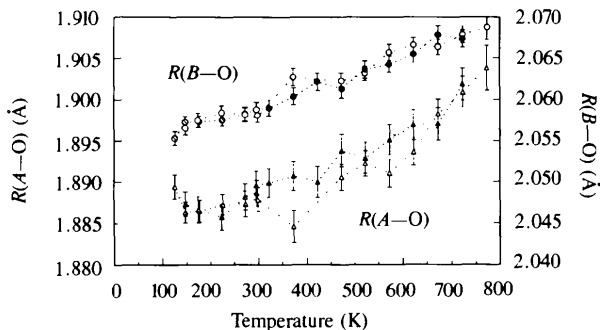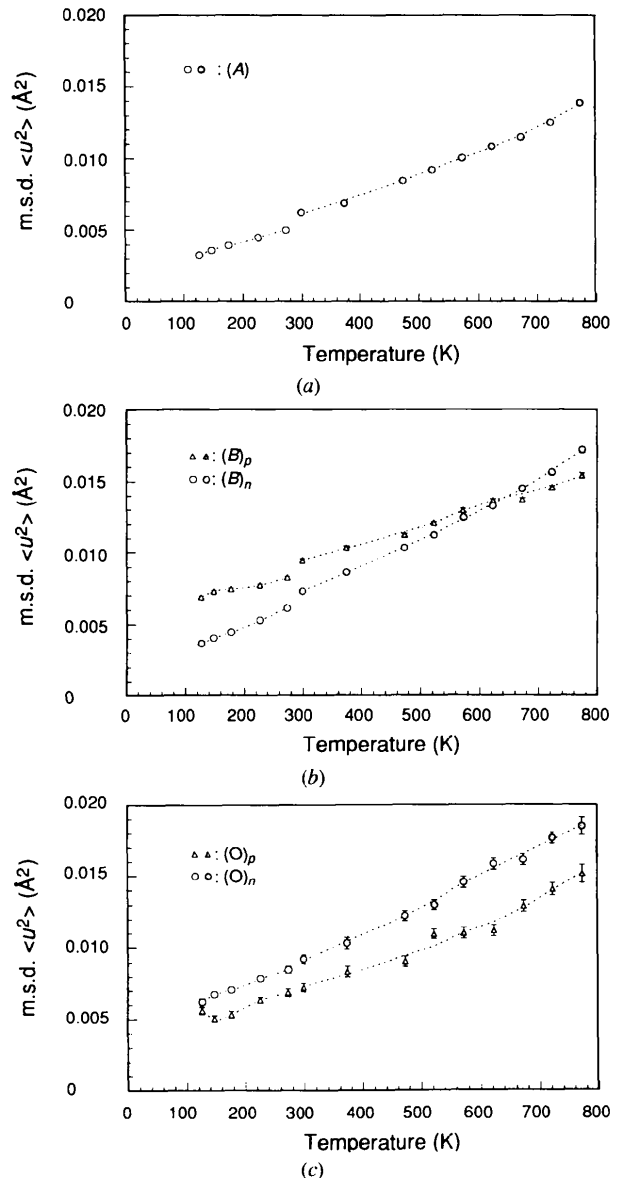

Fig. 4. Changes in bond distances R(*A*—O) and R(*B*—O). Slashed circles and triangles: cooling cycle on number 14; open circles and triangles: heating cycle on number 14; solid circles and triangles: cooling cycle on number 7; hatched circles and triangles: heating cycle on number 7. Error bars represent 1σ.

vibrational ellipsoids for the A and O atoms are as expected from librational motions of the AO_4 tetrahedra around the A atoms.

4.2. Oxygen coordinate, cation distribution and interatomic distances

As already mentioned, some *in situ* observations of spinels show a correlated change of i and x as a funciton of temperature. If the same type of correlation between i and x exists in magnetite, our observations on the variation of x indicate that the i value, not directly observed in the present study, in magnetite might be constant below ~600 K and decrease with increasing temperature above this value. This hypothesis is examined with reference to the observations for the thermal change of electron transport properties by Todo *et al.* (1995): we note an agreement between the temperatures, where x starts to increase and the electrical conductivity starts to deviate toward larger values than the linear temperature dependence. Todo *et al.* (1995) suggested that the occupation of the A site by Fe^{2+} at higher temperatures indicates the appearance of new n-type carriers in conduction bands which were empty at lower temperatures. Hence, the occupation of the A site by Fe^{2+}, in other words, a decrease in the i value, might cause the upward deviation of electrical conductivity. From a structural point of view, the hypothesis may be explained such that the increase of x is brought about by occupation of the A site by Fe^{2+} ions, *i.e.* disordering of Fe^{2+} ions over the A and B sites. Although the appearance of new carriers on the A site above ~400 K is suggested by Todo *et al.* (1995) from their thermal change data of the extraordinary Hall coefficient, effects of the disordering on both the bulk conductivity and x might be too small to be detected below 600 K.

At 299 K cation–anion distances $R(A—O)$ and $R(B—O)$ are 1.8878 (15) and 2.0581 (8) Å, respectively, and agree with the values reported by Fleet (1981)

within the e.s.d.'s. However, these values are all apparently different from those calculated using effective ionic radii, which were revised for the spinel structure (O'Neill & Navrotsky, 1983) and those calculated using the bond-valence scheme with parameters given by Brown & Altermatt (1985): $R(^{iv}Fe^{3+}—O) = 1.865$ Å and average of $R(^{vi}Fe^{2+}—O)$ and $R(^{vi}Fe^{3+}—O) = 2.073$–$2.078$ Å. These differences at room temperature, however, could not be ascribed to disorder over the A and B sites, if the magnetic moment of bulk crystals and results of spectroscopic studies such as Mössbauer spectroscopy (*e.g.* Kündig & Hargrove, 1969) are taken into consideration. FeO_6 octahedra in magnetite have clearly smaller $R(B—O)$ and only slightly smaller $R(B—B)$ than the corresponding values in a hypothetical 'ionic' magnetite ($a = 8.397$ Å and $x = 0.2532$), modeled using the ionic radii given by O'Neill & Navrotsky (1983). With respect to this contraction of FeO_6 octahedra, we note that the density of magnetite abruptly increases (Yoshida & Iida, 1979) at the transition from the low-temperature phase to the semimetallic high-temperature phase. Since $R(B—B)$ (2.967 Å at 299 K) is still larger than 2.95 Å, which is considered by Fleet (1982*b*) to be the critical cation–cation separation for electron delocalization, the deformation may suggest that electrons transfer between the B atoms *via* bridging oxygens, but not directly transfer between them.
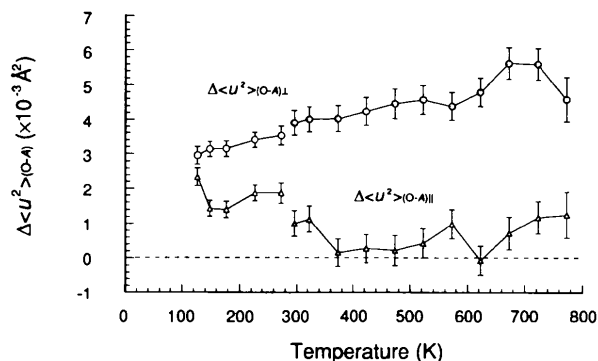
Fig. 6. Differences in m.s.d.'s at the A and O sites along and normal to the $A—O$ bond. Triangles: along $A—O$ ($<u^2>_{(O—A)\parallel}$); circles: normal to $A—O$ ($<u^2>_{(O—A)\perp}$). Open circles and triangles: cooling cycle on number 14; hatched circles and triangles: cooling cycle on number 7. Selected cycles are shown.

References

Becker, P. J. & Coppens, P. (1974). *Acta Cryst.* **A30**, 129–147.
Bond, W. L. (1960). *Acta Cryst.* **13**, 814–818.
Brown, I. D. & Altermatt, D. (1985). *Acta Cryst.* **B41**, 244–247.
Busing, W. R., Martin, K. O. & Levy, H. A. (1962). *ORFLS.* Report ORNL-TM-305. Oak Ridge National Laboratory, Oak Ridge, Tennessee, USA.
Coppens, P. & Hamilton, W. C. (1970). *Acta Cryst.* **A26**, 71–83.
Dieckmann, R. (1982). *Ber. Bunsenges. Phys. Chem.* **86**, 112–118.
Fleet, M. E. (1981). *Acta Cryst.* **B37**, 917–920.
Fleet, M. E. (1982*a*). *Acta Cryst.* **B38**, 1718–1723.
Fleet, M. E. (1982*b*). *J. Can. Ceram. Soc.* **51**, 13–15.
Fleet, M. E. (1986). *J. Solid State Chem.* **62**, 75–82.
Hamilton, W. C. (1958). *Phys. Rev.* **110**, 1050–1057.

Johnson, C. K. (1971). *ORTEP*II. Report ORNL-3794, revised. Oak Ridge National Laboratory, Tennessee, USA.

Johnson, C. K. & Levy, H. A. (1974). *International Tables for X-ray Crystallography*, edited by J. A. Ibers, & W. C. Hamilton, Vol. IV, pp. 311–336. Birmingham: Kynoch Press. (Present distributor Kluwer Academic Publishers.)

Kündig, W. & Hargrove, R. S. (1969). *Solid State Commun.* **7**, 223–227.

Marumo, F., Isobe, M. & Akimoto, S. (1977). *Acta Cryst.* **B33**, 713–716.

Morimoto, N., Tokonami, M., Watanabe, M. & Koto, K. (1974). *Am. Mineral.* **59**, 475–485.

O'Neill, H. St. C. & Navrotsky, A. (1983). *Am. Mineral.* **68**, 181–194.

Peterson, R. C., Lager, G. A. & Hitterman, R. L. (1991). *Am. Mineral.* **76**, 1455–1458.

Sharma, S. S. (1950). *Proc. Indian Acad. Sci. A*, **31**, 261–274.

Todo, S., Siratori, K. & Kimura, S. (1995). *J. Phys. Soc. Jpn*, **64**, 2118–2126.

Wu, C. C. & Mason, T. O. (1981). *J. Am. Ceram. Soc.* **64**, 520–522.

Yagi, T., Marumo, F. & Akimoto, S. (1974). *Am. Mineral.* **59**, 486–490.

Yamanaka, T. (1986). *Phys. Chem. Miner.* **13**, 227–232.

Yamanaka, T., Takéuchi, Y. & Tokonami, M. (1984). *Acta Cryst.* **B40**, 96–102.

Yoshida, J. & Iida, S. (1979). *J. Phys. Soc. Jpn*, **47**, 1627–1633.